LETTER

doi:10.1038/nature20147

A persistent and dynamic East Greenland Ice Sheet over the past 7.5 million years

Paul R. Bierman[1], Jeremy D. Shakun[2], Lee B. Corbett[1], Susan R. Zimmerman[3] & Dylan H. Rood[4,5]

Climate models show that ice-sheet melt will dominate sea-level rise over the coming centuries, but our understanding of ice-sheet variations before the last interglacial 125,000 years ago remains fragmentary. This is because terrestrial deposits of ancient glacial and interglacial periods[1–3] are overrun and eroded by more recent glacial advances, and are therefore usually rare, isolated and poorly dated[4]. In contrast, material shed almost continuously from continents is preserved as marine sediment that can be analysed to infer the time-varying state of major ice sheets. Here we show that the East Greenland Ice Sheet existed over the past 7.5 million years, as indicated by beryllium and aluminium isotopes (^{10}Be and ^{26}Al) in quartz sand removed by deep, ongoing glacial erosion on land and deposited offshore in the marine sedimentary record[5,6]. During the early Pleistocene epoch, ice cover in East Greenland was dynamic; in contrast, East Greenland was mostly ice-covered during the mid-to-late Pleistocene. The isotope record we present is consistent with distinct signatures of changes in ice sheet behaviour coincident with major climate transitions. Although our data are continuous, they are from low-deposition-rate sites and sourced only from East Greenland. Consequently, the signal of extensive deglaciation during short, intense interglacials could be missed or blurred, and we cannot distinguish between a remnant ice sheet in the East Greenland highlands and a diminished continent-wide ice sheet. A clearer constraint on the behaviour of the ice sheet during past and, ultimately, future interglacial warmth could be produced by ^{10}Be and ^{26}Al records from a coring site with a higher deposition rate. Nonetheless, our analysis challenges the possibility of complete and extended deglaciation over the past several million years.

Understanding of early Greenlandic glaciation remains fragmentary, uncertain and for some periods contradictory (Fig. 1 and references therein); much of what is known comes from marine sediment. The first presence of ice-rafted debris (IRD) at Ocean Drilling Program (ODP) site 918 suggests that East Greenland glaciers initially reached the coast about 7.5 million years (Myr) ago[6], whereas the surface texture of quartz at Site 918 suggests that glaciation there began 11 Myr ago[7]. IRD data suggest that the first large-scale glaciation of Greenland occurred in the latest Pliocene (3.3 Myr ago), and multiple IRD records indicate expansive Greenland glaciation by 2.7 Myr ago[8]. Poorly dated shallow marine deposits indicate periods of warmth in Greenland during the later Pliocene or early Pleistocene, some after the initial onset of glaciation[4]. Geochemical and pollen data suggest that southern Greenland was at least partially deglaciated and forested during Marine Isotope Stage (MIS) 11 (about 400,000 years (400 kyr) ago) and perhaps MIS 5e (about 130 kyr ago). In contrast, meteoric ^{10}Be data from silt at the base of the Greenland Ice Sheet Project 2 ice core (GISP2 in east-central Greenland) are consistent with continuous cover there by cold-based, non-erosive ice for millions of years[9], an assertion supported by noble gas measurements[10].

The concentration of cosmogenic nuclides in Earth materials reveals near-surface history[11,12]. In non-glaciated terrain, cosmic rays bombard Earth and produce ^{10}Be and ^{26}Al in mineral lattices. Production rates and nuclide concentrations decrease exponentially within a few metres of the surface; weak muon interactions continue at lower rates for tens of metres[13] (Fig. 2a). Covering a landscape with ice stops cosmogenic-nuclide production in the underlying rock. Subsequent glacial erosion first removes the most highly irradiated, near-surface material before excavating rock from depths containing progressively lower isotope concentrations (Fig. 2b).

Thermal conditions at the ice-sheet bed control its ability to erode, incorporate and transport rock and sediment. Warm-based ice (at the pressure melting point) can effectively erode rock and transport sediment to and off the coast[14]; thus, the isotopic record we present here is strongly biased towards areas of the ice sheet that were warm-based[15]. Cold-based ice, below the pressure melting point, is frozen to the bed and generally non-erosive[16]; it buries and preserves ancient landscapes rather than eroding them.

The ratio of the cosmogenic nuclides ^{10}Be and ^{26}Al provides additional information about burial after initial exposure[12]. Because ^{26}Al (half-life $t_{1/2} = 0.71$ Myr) radiodecays more rapidly than ^{10}Be ($t_{1/2} = 1.39$ Myr), burial of previously exposed material will, over time, lower both the ^{26}Al/^{10}Be ratio and the concentration of both isotopes (Fig. 2b). ^{26}Al and ^{10}Be are produced at a ratio of 7.3 ± 0.3 (1σ) near sea level and at high latitude in Greenland (Methods); thus, measured ^{26}Al/^{10}Be ratios falling below 7.3 are diagnostic of burial for long periods of time (more than about 200 kyr).

We measured cosmogenic-nuclide records spanning the last 7.5 Myr and 2.2 Myr at ODP sites 918 and 987, respectively (hereafter Site 918 and Site 987; Fig. 3; Extended Data Figs 1 and 2). Starting in the Miocene at Site 918, decay-corrected ^{10}Be concentrations generally decrease as sediment gets younger, reflecting the progressive glacial erosion of once-stable regolith and bedrock in East Greenland (Fig. 4c). Concentrations of ^{10}Be, corrected for radiodecay on the seafloor, are high (135,000 atoms per gram of quartz sediment) in the oldest glacial sediment[6] (about 7.5 Myr old; sample 918-30) and indicate that the pre-glacial East Greenland landscape was eroding at approximately 22 m per million years (Methods). As sediment and rock were removed from the landscape by glacial erosion, material that was deeply shielded in pre-glacial times, and thus less affected by cosmic radiation, was incorporated into basal ice and carried offshore. We infer that the decrease in ^{10}Be concentration was driven by glacial erosion because IRD at Site 918 and at other sites in East Greenland[2,5] indicates the presence of glaciers eroding rock, extending to the sea, and supplying the sand-sized sediment that we analysed[6]. A general increase in the intensity and spatial extent of glaciation after 7.5 Myr ago is supported by rising accumulation rates of coarse sediment over time at Site 918 (Fig. 4b)[6].

By the late Pliocene (around 3 Myr ago), when other records suggest that the first major ice expansion occurred over most of Greenland

[1]Department of Geology and Rubenstein School of the Environment and Natural Resources, University of Vermont, Burlington, Vermont 05405, USA. [2]Department of Earth and Environmental Sciences, Boston College, Chestnut Hill, Massachusetts 02467, USA. [3]Center for Accelerator Mass Spectrometry, Lawrence Livermore National Laboratory, Livermore, California 94550, USA. [4]Department of Earth Science and Engineering, Imperial College London, South Kensington Campus, London SW7 2AZ, UK. [5]Scottish Universities Environmental Research Centre, East Kilbride G75 0QF, UK.

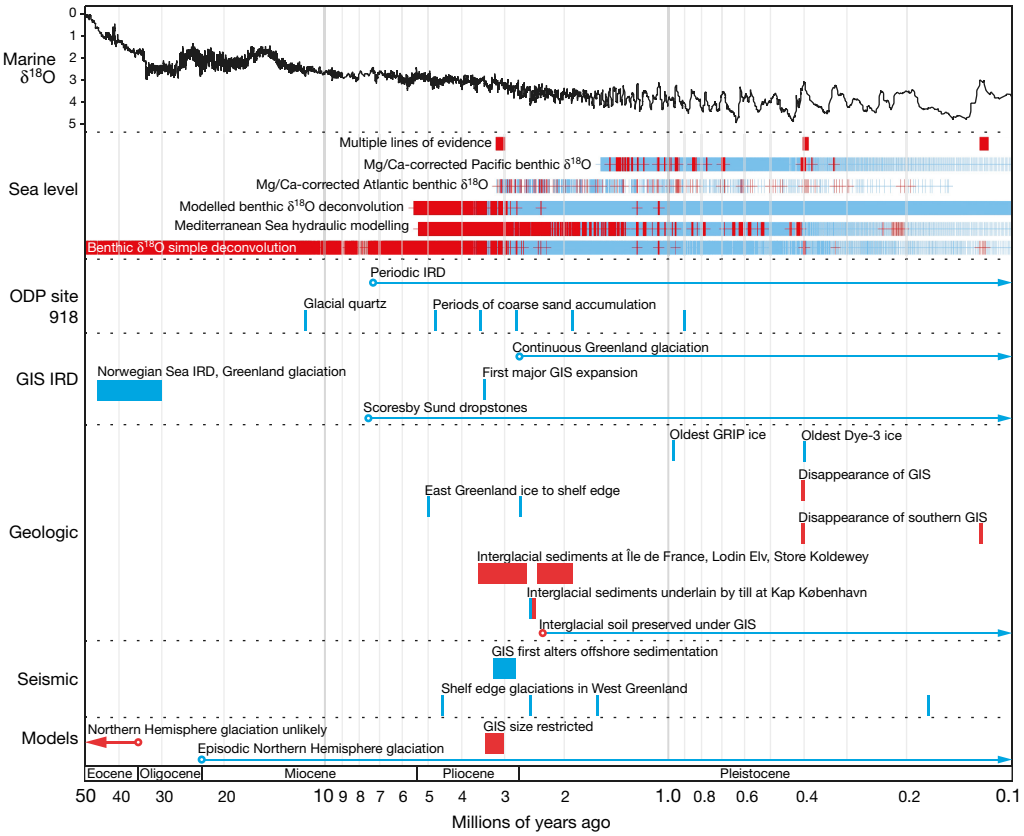

Figure 1 | Compilation of findings that constrain the long-term history of the GIS. Red indicates smaller ice sheet; blue indicates larger ice sheet. References for this figure are included in Extended Data Fig. 5. GRIP, Greenland Ice Core Project; Dye-3, an ice core named after the radar station where the core was collected.

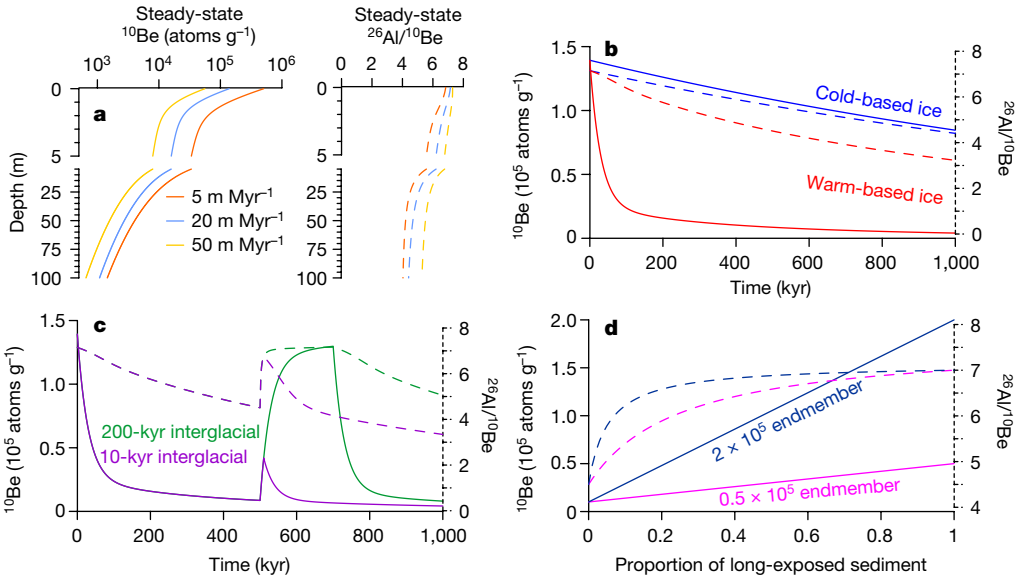

Figure 2 | Cosmogenic-nuclide systematics and sensitivity to erosion, burial, exposure and mixing. a, Estimated steady-state concentrations of ^{10}Be and the ^{26}Al/^{10}Be ratio as a function of depth below the preglacial surface of Greenland (sea level) for various erosion rates. **b**, ^{10}Be concentration (solid lines) and ^{26}Al/^{10}Be (dashed lines) starting from the 20 m Myr^{-1} steady-state profile following 1 Myr of cold-based ice cover and warm-based ice eroding at 20 m Myr^{-1}. **c**, ^{10}Be concentration (solid lines) and ^{26}Al/^{10}Be (dashed lines) (starting from the 20 m Myr^{-1} steady-state profile) following 1 Myr of warm-based ice eroding at 20 m Myr^{-1}, but interrupted by either a 10-kyr or 200-kyr interglacial exposure with 20 m Myr^{-1} erosion. **d**, ^{10}Be concentration (solid lines) and ^{26}Al/^{10}Be (dashed lines) of sediments mixed from varying proportions of an eroded and long-buried endmember (^{10}Be = 10,000 atoms g^{-1}; ^{26}Al/^{10}Be = 4.5) and two different long-exposed endmembers (^{10}Be = 50,000 atoms g^{-1}, 200,000 atoms g^{-1}; ^{26}Al/^{10}Be = 7.3 in both cases). Muon production rates in all panels were calculated using the MATLAB implementation in refs 13 and 28; see Methods for details.

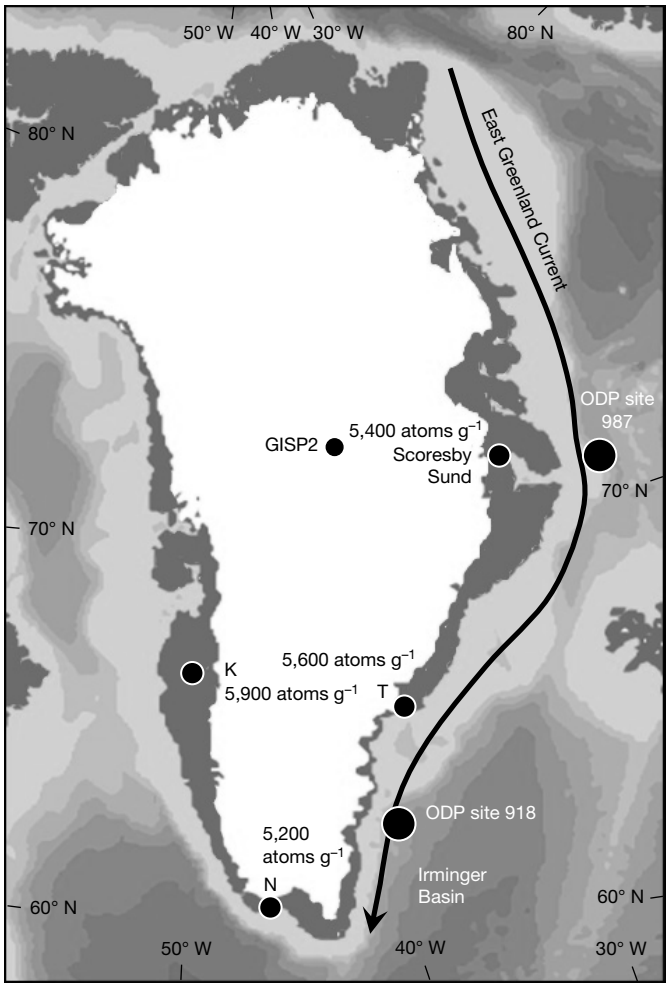

Figure 3 | Map of Greenland. ODP sites used in this study, the East Greenland Current, and locations where contemporary sediment samples were collected are shown. (K, Kangerlussuaq ($n = 26$); N, Narsarsuaq ($n = 16$); T, Tasilaq ($n = 12$); numbers give median ^{10}Be concentrations in these sediments[18] as well as a single value at Scoresby Sund[21].) Ocean bathymetry contoured in 500-m intervals; derived from MMap (https://www.eoas.ubc.ca/~rich/map.html). The locations of the GISP2 ice core site and Irminger Basin are shown.

(Fig. 1), decay-corrected ^{10}Be concentrations are more than an order of magnitude lower than at the beginning of the record, reaching a minimum of 12,000 atoms g^{-1} at 2.8 Myr. These data are consistent with warm-based glaciers having eroded parts of East Greenland for much of the Pliocene, and provide direct evidence for the model- and core-based supposition[8,17] that the Greenland Ice Sheet (GIS) has been present and eroding East Greenland since at least the Pliocene.

At the dawn of the Pleistocene, decay-corrected ^{10}Be concentration abruptly increases (Fig. 4c). Sediment deposited at around 2.5 Myr ago had about 140,000 atoms g^{-1} of ^{10}Be, more similar to Miocene-age (7.5-Myr-old) sediment than to any of Quaternary age (Supplementary Table 1). This ^{10}Be-rich quartz suggests early Pleistocene expansion of the ice sheet into previously unglaciated areas of East Greenland where stable Miocene regolith remained, an interpretation consistent with abundant IRD found at about 2.5 Myr both at Site 918[6] and elsewhere in the Arctic[8]. We suspect that this spike in ^{10}Be concentration does not represent an interglacial period, such as that indicated by the warm fauna and flora found in sediment of the Kap København Formation[4], because the interglacial represented by those sediments is thought to be short-lived (<20 kyr)[4]. Such a short duration is insufficient to raise ^{10}Be concentrations to the levels attained by continuous pre-glacial exposure[18] (Fig. 2c).

From 2.5 Myr to 0.8 Myr ago, the decay-corrected concentration of ^{10}Be generally declines (Fig. 4c), reflecting continued erosion of rock and regolith by warm-based areas of the eastern GIS. The decay-corrected ^{10}Be record at Site 918 shows parallels with core sedimentology (Fig. 4a, b); an overall inverse correlation exists between ^{10}Be concentration and sand content (Extended Data Fig. 3), and several previously noted IRD pulses line up with prominent drops in decay-corrected ^{10}Be concentration, such as pulses near 7 Myr, 2.8 Myr, 1.9 Myr and 0.8 Myr ago (Fig. 4b, c)[19]. These patterns are consistent with periods of intensified glacial erosion that excavated deeper-sourced material containing less ^{10}Be and delivered it offshore.

An abrupt, fourfold drop in ^{10}Be concentration occurs across the mid-Pleistocene transition at 0.8 Myr ago (Fig. 4c), a time when the duration and magnitude of glaciations increased[20]. This drop might reflect reduced interglacial exposure or increasing erosivity of the ice sheet. ^{10}Be concentrations over the past 0.8 Myr are similar to those in sediments issuing from the western, southern and eastern ice margin of Greenland today[18,21] (Figs 3 and 4c), except for one brief increase in a sample 400–200 kyr old. This higher concentration of ^{10}Be could reflect erosion of sediment exposed during the preceding long-lasting interglacial at MIS 11, a hypothesis supported by a slight, coincident rise in the ^{26}Al/^{10}Be ratio, consistent with interglacial re-exposure (Fig. 4c, d). With this exception, the consistently low ^{10}Be concentrations of the mid- to late Pleistocene sediment indicate the existence of a large, stable ice sheet in East Greenland for most of the past million years.

The shorter ^{10}Be record at Site 987 (2.2 Myr) is consistent with the latter part of the Site 918 record. Decay-corrected concentrations are steady and low at Site 987 (Fig. 4c, Supplementary Table 1), which suggests that IRD there was derived from glacial erosion of material that was deep below the land surface before East Greenland was ice-covered (Fig. 2a). Such efficient erosion of the former Miocene land surface is consistent with the location of Site 987 at the outlet of Scoresby Sund, a large fiord complex that is the major outlet for glaciers sourced in the highlands of East Greenland. Glacial erosion probably began early here because this part of East Greenland is thought to be where the ice sheet nucleated in the Late Miocene[6] and where it survived even the most extreme Pliocene warm periods[22]. That the ^{10}Be concentrations at Site 918 are fourfold higher during the early Pleistocene than at Site 987 suggests that at least some of the sediment delivered to Site 918 over this interval was sourced from southeast Greenland.

Decay-corrected ^{26}Al/^{10}Be data from Site 918 provide additional information about the history of Greenlandic sediment (Fig. 4d). The lack of correlation between ^{10}Be concentration and ^{26}Al/^{10}Be (Extended Data Fig. 4f) suggests that changes in the ^{26}Al/^{10}Be ratio are not driven by long periods of surface exposure, because such exposure would raise both the ratio and ^{10}Be concentration. This lack of correlation is, however, consistent with changing sediment source areas and erosion of material with different ^{26}Al/^{10}Be ratios. Changes in sediment source area may be driven by changes in the basal thermal regime of the ice sheet instead of, or in addition to, changes in ice extent. Spatial and temporal differences in ice-sheet behaviour probably drive where and when subglacial erosion occurs because remote sensing data show that areas of warm (erosive) and cold (non-erosive) ice are closely juxtaposed[23].

^{26}Al/^{10}Be does not decline steadily over time as would be expected if the entire source area of sediment had been completely and continually covered by ice, which would cause preferential loss of shorter-lived ^{26}Al (Fig. 4d). Rather, between 2.6 Myr and 1.7 Myr ago, the decay-corrected ^{26}Al/^{10}Be ratio (approximately 7.3) is mostly consistent with surface exposure. Decay-corrected ^{26}Al/^{10}Be ratios, similar to the production ratio, imply that ice did not cover the sediment source area for most of each glacial/interglacial cycle, because ^{26}Al/^{10}Be ratios change substantially only when surfaces are buried for several times longer than they are exposed and for at least several hundred thousand years in total[24]. In contrast, most of the Site 918 record that is younger than 1.4 Myr

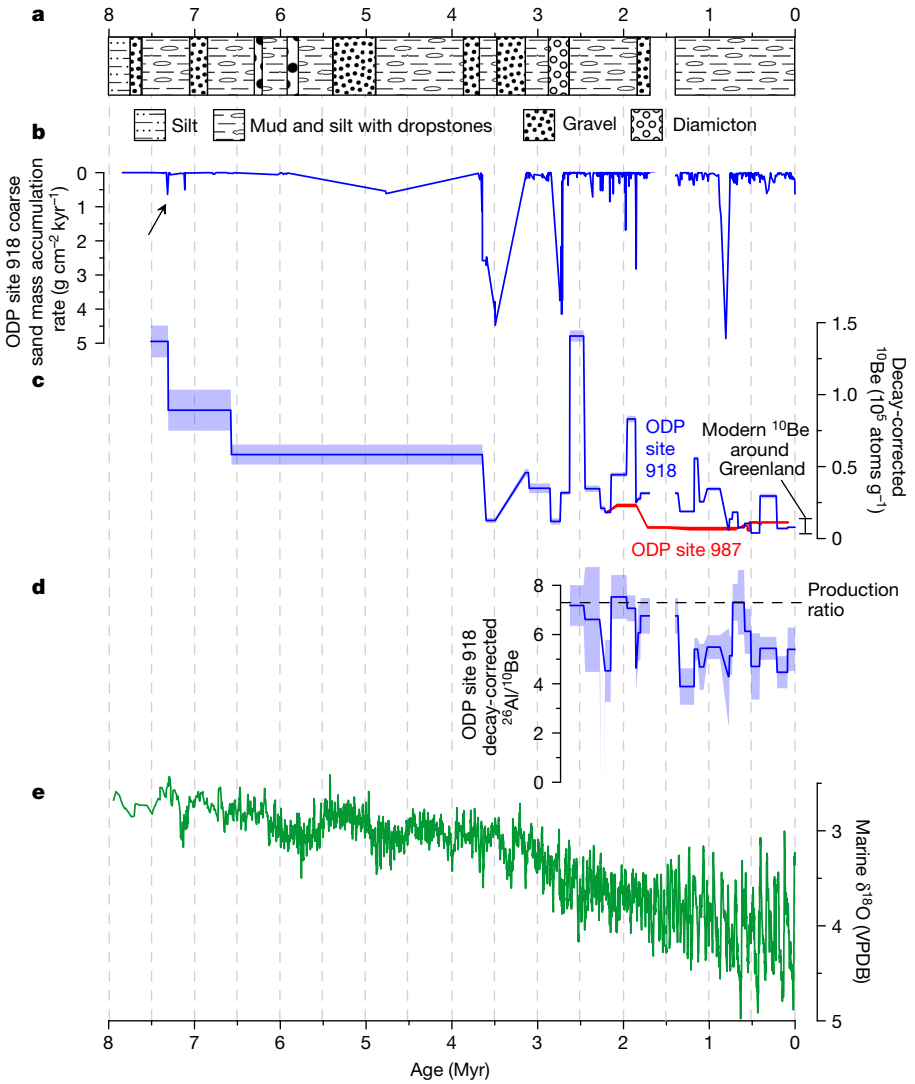

Figure 4 | Seven and a half million years of sediment cosmogenic-nuclide values from offshore East Greenland. a, Simplified lithostratigraphy at Site 918 (ref. 19). **b**, Coarse sand (0.25–2 mm) mass accumulation rate at Site 918 (ref. 19). Arrow indicates the oldest dropstones at the site[6]. **c**, Decay-corrected ^{10}Be concentrations at Sites 918 (blue, $n = 30$) and 987 (red, $n = 16$) with 1σ uncertainties. Black error bar shows the 1σ range of ^{10}Be in modern sediment ($n = 54$) from the Greenlandic margin[18]. **d**, Decay-corrected ^{26}Al/^{10}Be at Site 918 with 1σ uncertainty. **e**, Global marine δ^{18}O record[29]. Note hiatus arising from missing core section between 1.7 Myr and 1.4 Myr (**a**–**d**).

has decay-corrected ^{26}Al/^{10}Be ratios of around 5 with no decrease over time, which is consistent with the excavation of sediment mostly buried under ice. However, at least some of the material eroded from 1.4 Myr ago to the present must have been intermittently exposed during interglacials in order to prevent the ^{26}Al/^{10}Be ratio from falling steadily because of radiodecay. For a short period just after the mid-Pleistocene transition and the largest IRD spike (samples 918-6 and 918-7), the decay-corrected ^{26}Al/^{10}Be rises to about 7.3; we infer that the change in climate cyclicity allowed ice in East Greenland to expand into and erode areas that were not recently ice-covered.

The best hope for detecting short periods of deglaciation is the ^{26}Al/^{10}Be ratio. Contemporary Greenlandic river sand, both glacially and non-glacially sourced, has a ^{26}Al/^{10}Be ratio of 7.6 ± 2.1 (1σ, $n = 5$), which is probably the result of landscape re-exposure during substantial mid-Holocene retreat[25] (Supplementary Table 2). Sand deposited in the Keglen delta at Kangerlussuaq during the end of the last glaciation around 7 kyr ago[26] has a ^{26}Al/^{10}Be ratio of 4.54 ± 0.58, which is lower than the production ratio (Supplementary Table 2), and fully consistent with ratios we measured in marine cores over the last million years. Thus, high-precision ^{26}Al/^{10}Be ratio measurements of quartz extracted from a well dated, high-deposition-rate core may reveal glacial–interglacial cycles and could be used to better assess the lag time between exposure and marine deposition[27].

Cosmogenic isotopes preserved in marine sediment record progressive erosion of the pre-glacial landscape in East Greenland from about 7.5 Myr to 2.7 Myr ago, the first growth of a full ice sheet at about 2.5 Myr, and a change in ice-sheet behaviour at the 0.8-Myr-ago mid-Pleistocene transition. Measuring ^{26}Al with ^{10}Be demonstrates that erosion under the East GIS varied over time and space, and suggests that during the early and mid-Pleistocene, the ice sheet in East Greenland expanded into previously ice-free terrain. Considered along with isotopic measurements of contemporary Greenlandic sediment[18], the lack of repeated increases in ^{10}Be concentration or ^{26}Al/^{10}Be associated with interglacial periods during the past million years suggests that warming was sufficiently short-lived or modest that it seldom caused substantial and lengthy reductions in East GIS extent.

Online Content Methods, along with any additional Extended Data display items and Source Data, are available in the online version of the paper; references unique to these sections appear only in the online paper.

Received 10 February 2014; accepted 6 October 2016.

1. Nielsen, T. & Kuijpers, A. Only 5 southern Greenland shelf edge glaciations since the early Pliocene. *Sci. Rep.* **3,** 1875 (2013).
2. De Schepper, S., Gibbard, P. L., Salzmann, U. & Ehlers, J. A global synthesis of the marine and terrestrial evidence for glaciation during the Pliocene Epoch. *Earth Sci. Rev.* **135,** 83–102 (2014).
3. Gibbons, A. B., Megeath, J. D. & Pierce, K. L. Probability of moraine survival in a succession of glacial advances. *Geology* **12,** 327–330 (1984).
4. Funder, S. *et al.* Late Pliocene Greenland—the Kap København Formation in north Greenland. *Bull. Geol. Soc. Den.* **48,** 117–134 (2001).
5. Butt, A., Elverhøi, A., Forsberg, C. & Solheim, A. Evolution of the Scoresby Sund Fan, central East Greenland—evidence from ODP Site 987. *Norsk Geol. Tidskr.* **81,** 3–15 (2001).
6. Larsen, H. C. *et al.* Seven million years of glaciation in Greenland. *Science* **264,** 952–955 (1994).
7. Helland, P. E. & Holmes, M. A. Surface textural analysis of quartz sand grains from ODP site 918 off the southeast coast of Greenland suggests glaciation of southern Greenland at 11 Ma. *Palaeogeogr. Palaeoclimatol. Palaeoecol.* **135,** 109–121 (1997).
8. Flesche Kleiven, H., Jansen, E., Fronval, T. & Smith, T. M. Intensification of Northern Hemisphere glaciations in the circum Atlantic region (3.5–2.4 Ma) —ice-rafted detritus evidence. *Palaeogeogr. Palaeoclimatol. Palaeoecol.* **184,** 213–223 (2002).
9. Bierman, P. R. *et al.* Preservation of a preglacial landscape under the center of the Greenland Ice Sheet. *Science* **344,** 402–405 (2014).
10. Yau, A. M., Bender, M. L., Blunier, T. & Jouzel, J. Setting a chronology for the basal ice at Dye-3 and GRIP: implications for the long-term stability of the Greenland Ice Sheet. *Earth Planet. Sci. Lett.* **451,** 1–9 (2016).
11. Lal, D. Cosmic ray labeling of erosion surfaces; in situ nuclide production rates and erosion models. *Earth Planet. Sci. Lett.* **104,** 424–439 (1991).
12. Granger, D. E. A review of burial dating methods using ^{26}Al and ^{10}Be. *Spec. Pap. Geol. Soc. Am.* **415,** 1–16 (2006).
13. Heisinger, B. *et al.* Production of selected cosmogenic radionuclides by muons. *Geochim. Cosmochim. Acta* **66,** A558 (2002).
14. Elverhøi, A., Hooke, R. L. & Solheim, A. Late Cenozoic erosion and sediment yield from the Svalbard–Barents sea region: implications for understanding erosion of glacierized basins. *Quat. Sci. Rev.* **17,** 209–241 (1998).
15. Bell, R. E. *et al.* Deformation, warming and softening of Greenland's ice by refreezing meltwater. *Nat. Geosci.* **7,** 497–502 (2014).
16. Sugden, D. E. & Watts, S. H. Tors, felsenmeer, and glaciation in northern Cumberland Peninsula, Baffin Island. *Can. J. Earth Sci.* **14,** 2817–2823 (1977).
17. DeConto, R. M. *et al.* Thresholds for Cenozoic bipolar glaciation. *Nature* **455,** 652–656 (2008).
18. Nelson, A. H., Bierman, P. R., Shakun, J. D. & Rood, D. H. Using in situ cosmogenic ^{10}Be to identify the source of sediment leaving Greenland. *Earth Surf. Process. Landf.* **39,** 1087–1100 (2014).
19. John, K. E. K. S. & Krissek, L. A. The late Miocene to Pleistocene ice-rafting history of southeast Greenland. *Boreas* **31,** 28–35 (2002).
20. Lisiecki, L. & Raymo, M. A Pliocene-Pleistocene stack of 57 globally distributed benthic δ^{18}O records. *Paleoceanography* **20,** PA1003–PA1020 (2005).
21. Goehring, B. M., Kelly, M. A., Schaefer, J. M., Finkel, R. C. & Lowell, T. V. Dating of raised marine and lacustrine deposits in east Greenland using beryllium-10 depth profiles and implications for estimates of subglacial erosion. *J. Quat. Sci.* **25,** 1–10 (2010).
22. Hill, D. J., Dolan, A. M., Haywood, A. M., Hunter, S. J. & Stoll, D. K. Sensitivity of the Greenland Ice Sheet to Pliocene sea surface temperatures. *Stratigraphy* **7,** 111–122 (2010).
23. Petrunin, A. G. *et al.* Heat flux variations beneath central Greenland's ice due to anomalously thin lithosphere. *Nat. Geosci.* **6,** 746–750 (2013).
24. Bierman, P. R., Davis, P. T., Corbett, L. B., Lifton, N. & Finkel, R. Cold-based, Laurentide ice covered New England's highest summits during the Last Glacial Maximum. *Geology* **43,** 1059–1062 (2015).
25. Larsen, N. K. *et al.* The response of the southern Greenland ice sheet to the Holocene thermal maximum. *Geology* **43,** 291–294 (2015).
26. Storms, J. E. A., de Winter, I. L., Overeem, I., Drijkoningen, G. G. & Lykke-Andersen, H. The Holocene sedimentary history of the Kangerlussuaq Fjord-valley fill, West Greenland. *Quat. Sci. Rev.* **35,** 29–50 (2012).
27. DePaolo, D. J., Maher, K., Christensen, J. N. & McManus, J. Sediment transport time measured with U-series isotopes: results from ODP North Atlantic drift site 984. *Earth Planet. Sci. Lett.* **248,** 394–410 (2006).
28. Balco, G., Stone, J., Lifton, N. & Dunai, T. A complete and easily accessible means of calculating surface exposure ages or erosion rates from ^{10}Be and ^{26}Al measurements. *Quat. Geochronol.* **3,** 174–195 (2008).
29. Zachos, J., Pagani, M., Sloan, L., Thomas, E. & Billups, K. Trends, rhythms, and aberrations in global climate 65 Ma to present. *Science* **292,** 686–693 (2001).

Supplementary Information is available in the online version of the paper.

Acknowledgements Research supported by NSF ARC-1023191. A. Nelson prepared some samples. W. Hale and the Bremen Core Repository facilitated core sampling. G. Balco provided input on muon production. We thank K. St John for providing ODP site 918 mass accumulation rate data, B. de Boer for ice sheet model output, W. Huang for running foraminifer stable isotope samples, and S. Xu and the staff of the SUERC AMS laboratory for support during ^{26}Al measurements. This is LLNL-JRNL-701099.

Author Contributions P.R.B. and J.D.S. designed the experiment. J.D.S. oversaw core sampling. P.R.B. and L.B.C. did and oversaw laboratory work. D.H.R., S.R.Z. and P.R.B. performed isotopic analyses. P.R.B., J.D.S., L.B.C. and D.H.R. interpreted the data and all authors contributed to the preparation of the paper.

Author Information Reprints and permissions information is available at www.nature.com/reprints. The authors declare no competing financial interests. Readers are welcome to comment on the online version of the paper. Correspondence and requests for materials should be addressed to P.R.B. (pbierman@uvm.edu).

Reviewer Information *Nature* thanks D. Dahl-Jensen, D. Granger and the other anonymous reviewer(s) for their contribution to the peer review of this work.

METHODS

Hypothesis testing. We use new isotopic data, in conjunction with sensitivity tests, a forward model, and other extant records, to evaluate three hypotheses about the behaviour of the East GIS that previous data have not been able to address conclusively. For the past 7.5 Myr, we test whether (1) East GIS behaviour mirrored global climate/ice volume as represented by the marine $\delta^{18}O$ record; (2) the efficacy of erosion under the East GIS varied over time and space; (3) most interglacial periods were sufficiently short-lived or cool enough that they did not cause notable reductions in East GIS extent.

Compilation of deep time history of the GIS. Most of what is known about long-term ice-sheet history comes from marine sediment records interpreted as global or regional proxies for ice volume or glacial activity. For example, stable oxygen isotope measurements of foraminifera isolated from marine sediment track global ice volume and ocean temperature, but provide little information about the individual behaviour of each of the world's major ice sheets[20]. Global sea-level history reflects total ice volume, but in a complex fashion[30] because the record is aliased by local tectonic and glacio-isostatic adjustment of land levels[31]. The most robust inferences about the comings and goings of now-vanished ice sheets are based on the presence and provenance in marine sediment of IRD shed from melting icebergs that originated on glaciated continents[2,8]. IRD records are illustrative of when sediment-bearing glacial ice reached the coast, but with few exceptions[32] do not otherwise constrain ice extent[33]. Figure 1 presents our compilation of references relevant to understanding the history of ice on Greenland since the Miocene. References for Fig. 1 are cited in Extended Data Fig. 5.

Determining sediment source area. Making accurate inferences about ice-sheet behaviour on the basis of terrestrial sediment recovered from marine archives requires knowledge of the sediment source area. Multiple lines of evidence indicate that the quartz we isolated was sourced from East Greenland. The East Greenland Current (Fig. 3) drifts icebergs from north to south over both Sites 918 and 987, which suggests that the IRD we analysed is dominantly from East Greenland[34]. IRD composition downcore at Site 918 consistently indicates eastern Greenland sediment sourcing for millions of years[35–37]. While there may be some contribution from gravity flows off the continental shelf, sedimentological evidence suggests that most sand at Site 918 comes from ice rafting rather than turbidites[6,19,38,39]. At Site 918, sand is compositionally similar to larger dropstones, which is consistent with an IRD source for the sand[40]. Sediment at Site 987 is probably more locally sourced because drilling was done on the toe of a large subaqueous fan[5]; although some of the Site 987 sediment may come from the north, most was presumably delivered directly from ice flowing east through Scoresby Sund (Fig. 3). In summary, the cosmogenic data we present reflect the history of and processes active in eastern Greenland.

Thermal conditions at the base of the ice sheet are not well known and change over time[41] and space[23,42]. Warm-based ice (the ultimate source of the sediment we analysed because it is required to erode the material) is most likely to be found in deep troughs, near some ice margins, and where geothermal heat flux is high[23,43,44]. Models suggest that 20% to 30% of the pre-industrial Holocene GIS was warm-based[43], but during the Last Glacial Maximum up to 50% of ice on Greenland may have been warm-based, perhaps due to increased thickness[41].

Paired $^{26}Al/^{10}Be$ approach and the $^{26}Al/^{10}Be$ production ratio of 7.3. Because cosmogenic nuclides with different half-lives decay at different rates after production ceases, multiple nuclides can be measured in tandem (for example, ^{10}Be and ^{26}Al) to provide insight about periods of burial. A multi-nuclide approach can thus constrain the timing and duration of burial by non-erosive, cold-based ice[45], which is a process that has probably occurred variably in Greenland over both space and time.

When exposure begins on a fresh surface, the $^{26}Al/^{10}Be$ ratio is the production ratio of the two nuclides. If a previously exposed surface is buried and shielded from further nuclide production, the $^{26}Al/^{10}Be$ ratio drops because the 0.71-Myr half-life of ^{26}Al (ref. 46) is shorter than the 1.39-Myr half-life of ^{10}Be (refs 47–49). If a sample is exposed again following burial, production resumes and the $^{26}Al/^{10}Be$ ratio increases because the production rate of ^{26}Al is greater than that of ^{10}Be. It is important to note that relatively short burial durations (<100–200 kyr) and/or re-exposure following burial can result in $^{26}Al/^{10}Be$ ratios that are indistinguishable from the production ratio[24,50] even though the surface has experienced periods of burial lasting tens of thousands of years.

Any inferences stemming from $^{26}Al/^{10}Be$ ratios are largely dependent upon the assumed $^{26}Al/^{10}Be$ production ratio, which is a direct function of the production rates of the two nuclides. Although nuclide production rates have long been known to vary across latitude and elevation[11,51], it has generally been assumed that ^{10}Be and ^{26}Al production rates scale similarly, with a resulting production ratio of 6.75 for all locations on Earth's surface[28]. However, recent work has suggested that the production ratio is itself dependent on latitude and elevation because each isotope's production rate scales differently across space[52–54]. Argento *et al.*[52] used numerical models to estimate a $^{26}Al/^{10}Be$ production ratio of 7.0 to 7.1 at sea level and high latitude, which is in agreement with the median value of 7.16 calculated from low-elevation (<2,000 m) calibration samples presented in the same study. Sites from a range of latitudes and elevations have production ratios ranging from 7.0 to 7.3, scaled to sea level and high latitude, and using seven different scaling schemes[54]. Atmospheric mass drives the differences in production between nuclides, with elevation probably being more important than latitude[55], although comprehensive studies of the global variation in the $^{26}Al/^{10}Be$ production ratio have not yet been conducted.

In this study, we place more emphasis on the relative rather than the absolute $^{26}Al/^{10}Be$ ratio in marine sediment over time; hence the assumed $^{26}Al/^{10}Be$ production ratio is less important here than in studies inferring absolute exposure and burial durations. However, we base our assumed production ratio on the work of Corbett *et al.*[56], who quantified $^{26}Al/^{10}Be$ in 24 continuously exposed bedrock and boulder surfaces at four high-latitude sites in Greenland that were deeply eroded during the last glaciation. They determined a $^{26}Al/^{10}Be$ production ratio of 7.3 ± 0.3 (slope of a York linear regression fit to all data with errors in both variables, 1σ), supporting recent modelling work indicating that the production ratio can exceed 6.75 at locations such as Greenland. Although the geographic variability of the production ratio is still unclear, we choose to employ the production ratio of ref. 56 here because the source of the sediments from Sites 918 and 987 is similar to the latitude range of the calibration samples in their data set.

Sample measurements. We measured ^{10}Be in 30 samples and ^{26}Al in 22 samples spanning the last 7.5 Myr and 2.6 Myr, respectively, in sediment cores at Site 918, located in the Irminger basin 110 km southeast of Greenland (63.1° N, 38.6° W, 1,800 m water depth). This site was previously used to define the onset of Greenland glaciation on the basis of the earliest occurrence of IRD[6], which is included in our oldest sample. We also measured ^{10}Be in 16 samples from Site 987 spanning the last 2.2 Myr of deposition 130 km offshore of Scoresby Sund and 1,200 km northeast of Site 918 (70.5° N, 17.9° W, 1,670 m water depth)[57].

Core samples were obtained from the Bremen Core Repository. We disaggregated and wet-sieved sediments isolating the grain size fraction 0.125–0.750 mm and used weak acid ultrasonic leaching (0.25% to 0.5% HF and HNO_3) to slowly dissolve all minerals other than quartz[58]. We amalgamated quartz from subsamples taken over an interval of core until we had sufficient quartz mass (7.8 g to 25.3 g) from which to extract and reliably measure ^{10}Be. Thus, samples represent the average ^{10}Be content of quartz present in core sections ranging in length from 0.04 m to 91 m (median 6 m, standard deviation 19 m). All uncertainties reported in this paper are 1σ.

Age spans for samples range from 0.001 Myr to 2.9 Myr (median 0.1 Myr, standard deviation 0.5 Myr). Our marine sediment record of ^{10}Be and ^{26}Al concentrations does not have the temporal resolution to clearly reflect major high-frequency changes in Plio-Pleistocene climate, such as the major interglacials at MIS 11, MIS 9 or MIS 5e. The need to amalgamate sufficient quartz for measuring very low isotope abundances meant that integration of core sediment over depth (and thus time) mixed sand deposited during glacial and interglacial periods; analysis of a core more proximal to the continental shelf might overcome this limitation.

After purifying quartz, samples were dissolved using HF in the presence of ^{9}Be carrier produced from beryl. Samples were processed in batches of 12 including two full chemistry process blanks[59]. ^{10}Be measurements were made at the Center for Accelerator Mass Spectrometry at Lawrence Livermore National Laboratory[60,61] and referenced to standard 07KNSTD3110 (ref. 46) assuming a $^{10}Be/^{9}Be$ ratio of $2{,}850 \times 10^{-15}$. ^{26}Al measurements were made at the Scottish Universities Environmental Research Centre[62] and normalized to the Z92-0222[46] standard with a nominal $^{26}Al/^{27}Al$ ratio of 4.11×10^{-11}. The average blank ratio ($^{10}Be/^{9}Be = (4.6 \pm 1.0) \times 10^{-16}$, $n = 6$; group 1, $^{26}Al/^{27}Al = (8.5 \pm 2.1) \times 10^{-16}$, $n = 4$; group 2 $^{26}Al/^{27}Al = (14.9 \pm 4.5) \times 10^{-16}$, $n = 4$) was subtracted from measured ratios, and uncertainties in sample and blank ratios were propagated in quadrature (Supplementary Table 1).

Replicate preparation of sample 918-17 (918-17X) indicates reproducibility within measurement uncertainty (Supplementary Table 1). Statistically identical measured concentrations of ^{10}Be in four samples (987-E to 987-H) collected from different depths in a 70-cm-thick IRD-rich layer ($4{,}250 \pm 370$ to $4{,}460 \pm 300$ atoms g^{-1}) also demonstrate the reproducibility of our measurements (Supplementary Table 1).

In all samples, measured ^{10}Be concentrations are low (2,100 to 40,000 atoms g^{-1}), but well above procedural backgrounds. Because of the shorter half-life of ^{26}Al, it is detectable only in younger samples (<2.6 Myr), and was measured only at Site 918; concentrations of ^{26}Al are also low (9,700 to 118,000 atoms g^{-1}; Supplementary Table 1), but similarly well above background. Cosmogenic $^{26}Al/^{10}Be$ ratios at the time of deposition (corrected by core depth–age models) range from about 3.9 to about 7.5 (Supplementary Table 1).

Age models for Sites 918 and 987 and decay-correction procedure. For Site 918, we used established age–depth constraints from ref. 19, who applied ages from the timescale of ref. 63 to magnetostratigraphic[64] and biostratigraphic datums[65,66]. Ages were linearly interpolated between these control points (Extended Data Fig. 1). Note that there is an erosional hiatus at 71.1 m below the seafloor, which is estimated to span 1.71–1.39 Myr[19]. We also developed a planktonic $\delta^{18}O$ record (*N. pachyderma*, left-coiling) to refine the age model above the Brunhes–Matuyama reversal (780 kyr) at 45.9 m below the seafloor[64]. 168 stable isotope measurements were made at the Lamont–Doherty Earth Observatory, and 11–15 tests were used per sample. The $\delta^{18}O$ record clearly displays the Holocene and the last interglacial, but there is some ambiguity in the identification of other marine isotope stages, such as MIS 11 and MIS 13 (Extended Data Fig. 2).

For Site 987, we developed an age model by linearly interpolating between the age control points reported by the Leg 162 shipboard scientific party[57], which are primarily based on palaeomagnetic events (Extended Data Fig. 1).

Measured ^{10}Be and ^{26}Al concentrations (Supplementary Table 1) were corrected for decay since deposition on the seafloor using these age models and assuming half-lives of ^{10}Be $t_{1/2} = 1.39$ Myr (ref. 49) and ^{26}Al $t_{1/2} = 0.71$ Myr (ref. 67). Since our cosmogenic-nuclide samples were amalgamated from subsamples spanning 0.001 Myr to 2.9 Myr (Supplementary Table 3), we used the sand mass-weighted mean age of these subsamples to derive a single integrated age for each cosmogenic sample. Age model uncertainties can alter the absolute value of decay-corrected ^{10}Be concentrations and change the timing of some isotopic shifts, but have minimal impact on the overall structure of the record.

Sensitivity tests. We examined the sensitivity of ^{10}Be concentrations and $^{26}Al/^{10}Be$ ratios to erosion, burial, exposure and mixing (Fig. 2), assuming sea-level high-latitude production rates, including production from muons calculated using the MATLAB implementation[13,28]. Depth profiles were first run to secular equilibrium, which was reached when nuclide production balanced loss via radiodecay and erosion; the latter was simulated by shifting the profile upward each time step in proportion to the prescribed ice-free surface erosion rate (5 m Myr^{-1}, 20 m Myr^{-1} or 50 m Myr^{-1}). Steady-state profiles with higher erosion rates have lower ^{10}Be concentrations because nuclides are shed more rapidly, but they have higher $^{26}Al/^{10}Be$ ratios because nuclides are brought to the surface more quickly and thus have less time to decay in the subsurface (Fig. 2a). We simulated cold-based ice cover for 1 Myr by halting production and allowing the 20 m Myr^{-1} steady-state profile to decay in place without additional sub-ice erosion, whereas an analogous simulation for warm-based ice cover continued to erode under ice at 20 m Myr^{-1}. Surface nuclide concentrations decrease much faster under the erosive warm-based ice, and $^{26}Al/^{10}Be$ ratios also decline more quickly since the erosive ice brings deeper-buried (and thus longer-buried) nuclides to the surface. The 1-Myr-long warm-based ice simulation was performed again, but interrupted by either a 10-kyr or 200-kyr episode of interglacial exposure (with ice-free surface erosion continuing at 20 m Myr^{-1}) halfway through the simulation. In these simulations, because nuclide concentrations were very low before the interglacials, both were able to quickly reset the $^{26}Al/^{10}Be$ ratio to pre-glacial values; however, only the very long (200 kyr) interglacial had sufficient time to fully rebuild nuclide concentrations. Lastly, we modelled the mixing of sediment from low-concentration, low-ratio (eroded and long-buried) and high-concentration, high-ratio (long-exposed) endmembers to understand how the values we measured in marine sediments might reflect contributions from multiple source areas on Greenland. Nuclide concentrations mix linearly: $C_{mixed} = C_1F_1 + C_2F_2$, where C_1 and C_2 and F_1 and F_2 are the nuclide concentrations and mixing fractions ($F_1 + F_2 = 1$) of the two endmembers. $^{26}Al/^{10}Be$ ratios, however, exhibit nonlinear mixing that is weighted by the ratio of the endmembers' nuclide concentrations, because the greater the number of nuclides one endmember contributes relative to the other, the more it influences the mixed nuclide ratio: $R_{mixed} = R_1(C_1F_1/(C_1F_1 + C_2F_2)) + R_2(C_2F_2/(C_1F_1 + C_2F_2))$.

Our sensitivity tests demonstrate how progressively deeper erosion, interglacial exposure, burial by cold-based ice, and sediment mixing from different sources affect the concentration of ^{10}Be and ^{26}Al in terrestrial sediment exported from Greenland (Fig. 2). Such modelling shows that covering a landscape with non-erosive, cold-based ice for hundreds of thousands of years lowers the $^{26}Al/^{10}Be$ ratio, but does not much change ^{10}Be concentration because of the long half-life of ^{10}Be in relation to the burial duration (Fig. 2b). In contrast, cover by erosive, warm-based ice not only lowers the $^{26}Al/^{10}Be$ ratio by shielding the bed from cosmic ray exposure, but also lowers nuclide concentrations because it erodes material with previously produced nuclides and incorporates rock or sediment that was once deeply shielded from cosmic radiation. After the upper several metres of rock and soil are eroded by warm-based ice, isotopic concentrations in the resulting sediment are low and relatively insensitive to continued erosion. This is because the concentration of ^{10}Be in sediment produced by glaciers is controlled primarily by the extent of sub-ice erosion into the deep, muon-dominated production zone that extends tens of metres below the pre-glacial land surface where nuclide concentration changes only gradually with depth (Fig. 2a). When sediment is the result of mixing of components with different burial and erosion histories, the history of the sediment may be constrained by considering possible end members with different nuclide concentrations and $^{26}Al/^{10}Be$ ratios, mixed in different proportions (Fig. 2d). The ^{10}Be concentrations we measured reflect the erosion-weighted average ^{10}Be concentration of the areas from which they were sourced, while $^{26}Al/^{10}Be$ ratios are biased towards source areas that had relatively high nuclide concentrations.

^{10}Be and ^{26}Al concentrations measured in contemporary terrestrial Greenlandic sediment. To better constrain the interpretation of cosmogenic-nuclide measurements in marine sediment, we collected sediment samples from Greenlandic rivers, moraines and river terraces and measured their ^{10}Be (ref. 18), and in some cases, ^{26}Al concentrations (Supplementary Table 2). Sediment sourced from the ice sheet in eastern, western and southern Greenland both today[18] and at the end of the last glaciation (sampled in well-dated terraces)[18,21] has very low concentrations of ^{10}Be of only thousands of atoms per gram. Sediment in streams draining only areas outside the current ice margin has on average several times more ^{10}Be, which reflects exposure of the land surface to cosmic radiation during the Holocene[18]. Isotope and mass balance calculations indicate that most sediment now being delivered to the Greenlandic margin originates from beneath the ice sheet and not from the deglaciated margin[18].

To complement existing ^{10}Be data[18], we measured ^{26}Al in four samples of contemporary river sediment as well as sediment from the Keglen Delta terrace at Kangerlussuaq[26] (sample GLX-08) and another terrace deposited near Narsarsuaq[68] (GLX-34). Sediment in the Keglen Delta was deposited during the deglaciation (about 7 kyr ago)[26] and has a $^{26}Al/^{10}Be$ ratio substantially lower than the production ratio (GLX-08, 4.54 ± 0.58, 1σ). All sediment from modern streams, as well as that in the terrace at Narsarsuaq (GLX-34) deposited during a neoglacial readvance about 1.5 kyr (after mid Holocene retreat and exposure of the now mostly ice-covered landscape)[68], has an average ratio of 7.62 ± 2.12 (1σ; $n = 5$), similar to the production ratio. These data imply that at deglaciation, sediment leaving the ice sheet about 7 kyr ago had an $^{26}Al/^{10}Be$ ratio lower than the production value, and that exposure during the mid-Holocene, when the GIS retreated a few to tens of kilometres inland of the current margin, raised the $^{26}Al/^{10}Be$ to or near that of production, as suggested by our sensitivity tests (Fig. 2).

These results imply that short periods (about 10–20 kyr) of subaerial interglacial exposure, primarily at the margins of the ice sheet, matter little because they change the nuclide concentration substantially only in the uppermost few metres of rock or soil via shallow neutron spallation reactions. However, even short interglacial re-exposure can effectively raise the $^{26}Al/^{10}Be$ ratio if initial nuclide concentrations are very low when exposure begins (Fig. 2c).

Inherent method limitations. The glacial sediment system itself may limit the resolution of the record. Sediment tracing using ^{10}Be unambiguously shows that most sediment delivered to the current-day Greenland margin during the Holocene interglacial is derived from under the ice, has very little ^{10}Be and ^{26}Al, and is not sourced from the deglaciated peripheral area[18]. Sediment currently being shed from deglaciated terrain has concentrations of ^{10}Be several times higher than that of glacially derived material, but the marginal area is small in comparison to the area still covered by ice[18]. During glacial advances, sediment from previously exposed margins will be incorporated by ice and eventually mixed with long-shielded material and moved offshore. Even though the marginally sourced material has higher concentrations of ^{10}Be, it is overwhelmed volumetrically by material coming from areas that have been long covered by ice and thus limits the marine record's sensitivity to interglacial cosmic-ray exposure.

Calculation of background, pre-glaciation erosion rate for East Greenland. We determined a pre-glacial erosion rate for southeast Greenland from the decay-corrected ^{10}Be concentration in our oldest sample at Site 918 ($135{,}000 \pm 10{,}900$, 1σ; Supplementary Table 1), which integrates sediments from the 20 m of core immediately below the oldest dropstone at Site 918 identified by ref. 6. Assuming the ^{10}Be in this sample was produced at the surface at sea level directly onshore from Site 918 and experienced no topographic shielding, we obtain an erosion rate of approximately 22 ± 3 m Myr^{-1} using the CRONUS calculator v.2.3[28]. This estimate is relatively insensitive to these assumptions, except for elevation, which would, for instance, double the erosion rate if production occurred at 1,000 m above sea level rather than at sea level.

Site 918 ^{10}Be comparison to core sand content. We measured Site 918 sand (>63 μm) content and binned data over the same depth intervals as the ^{10}Be samples to facilitate comparison. We similarly binned values in the marine benthic $\delta^{18}O$ record[29] over the same time intervals as the Site 918 ^{10}Be record. Regressions, using logarithmic scaling for the Site 918 ^{10}Be and sand records, show pronounced

relationships, with lower ^{10}Be associated with higher sand content and more enriched marine δ^{18}O ($r^2 = 0.52$ in both cases, $P < 0.001$) (Extended Data Fig. 3). As Site 918 sand concentrations probably reflect glacial erosion on land and marine δ^{18}O is a proxy for global ice volume, these relationships are broadly consistent with intensified glacial activity yielding lower ^{10}Be concentrations in East-Greenland-derived sediments.

Forward modelling and code availability. As a first-order attempt to reproduce the Sites 918 and 987 cosmogenic-nuclide records, we constructed a simple model of GIS dynamics and cosmogenic-nuclide concentrations driven by three different plausible ice volume reconstructions over the past 5.3 Myr. The model consists of two sets of ten parallel cosmogenic-nuclide depth profiles, as described in Methods section 'Sensitivity tests', and was initialized using 20 m Myr^{-1} ice-free surface erosion rate steady-state nuclide depth profiles reflecting pre-ice-sheet conditions as indicated by the deepest sample in Site 918. Ice sheet extent was modelled from 0% to 100% in 10% increments by turning nuclide production on or off for the corresponding number of depth profiles at a given time step; for example, production was on for all depth profiles when ice cover was 0%, but for only nine profiles when ice cover was 10%, and so on. The time step is 2 kyr. Since the actual GIS extent through time is poorly constrained, we tried parameterizing it with three different time series: a sea-level record derived from δ^{18}O variations in the semi-enclosed Mediterranean Sea basin[69], the marine δ^{18}O record of global ice volume and deep ocean temperature[20], and a simulated history of the GIS from an ice-sheet model forced by the marine δ^{18}O record[70]. The last time series explicitly gives ice-sheet extent; the relationship between the first two series and GIS extent was calibrated by assuming that ice cover was 100% at 12 kyr, 80% today, 50% during MIS 11, 20% during the mid-Pliocene, and 0% in the Miocene.

We used a simple formulation of basal temperature regimes beneath the modelled ice. Because the GIS has roughly equal areas of cold- and warm-based ice today[44], we set the modelled ice cover also to have equal fractions by making one set of depth profiles warm-based (sub-ice erosion rate 20 m Myr^{-1}) and the other set cold-based (sub-ice erosion rate 0 m Myr^{-1}). Spatial variability in basal temperature regimes was introduced by switching between the warm-based and cold-based regime of the two sets of depth profiles every 500 kyr; this is not meant to be realistic, but rather simply to help assess the role of this variable in driving cosmogenic-nuclide concentrations given that the basal thermal history of the GIS is not known. Erosion rates were 20 m Myr^{-1} in ice-free areas. The simulated cosmogenic-nuclide values shown in Extended Data Fig. 4 represent the material shed from ice-covered, warm-based depth profiles in the model, and assume instantaneous transport to the deep sea.

This forward modelling illustrates the limitations in the approach we present here as well as the uncertainty of assumptions underlying the model (Extended Data Fig. 4). Our model reproduces the overall ^{10}Be record for both Sites 918 and 987, but does not capture the fine structure of the Site 918 data. The ice-sheet extent from a model simulation[70] consistently underestimates ^{10}Be and ^{26}Al/^{10}Be, probably because it does not accurately reflect GIS dynamism in the Pleistocene. The marine δ^{18}O proxy[20] and sea-level proxy[69] generate more realistic ^{26}Al/^{10}Be; the sea-level proxy generates the best fit to the ^{10}Be record. We interpret the fine structure (^{10}Be peaks at 2.5 Myr, 1.9 Myr and 1.1 Myr), which we cannot model, as changes in the sediment source area to which cosmogenic nuclides are singularly sensitive; most likely these peaks represent expansion of warm-based areas of the ice sheet into terrain that had not previously been eroded.

The MATLAB code files used to generate the forward model are available at https://github.com/shakunj/Bierman-et-al-2016-Nature. The three versions of the model are provided as MATLAB code files with the forcing series representing GIS extent through time designated in the model file name (*forward_model_XXXXX.mat*). These input driving series are the deep-sea δ^{18}O record[20] (*LR04.mat*), the Mediterranean Sea sea-level record[69] (*med.mat*), and simulated ice sheet extent based on modelling[70] (*deboer.mat*), all given at 2-kyr resolution over the past 5.3 Myr. Initialized bedrock profiles with steady-state ^{10}Be and ^{26}Al concentrations at 1-cm depth increments below the surface assuming a sea-level high-latitude production rate and 20 m Myr^{-1} ice-free surface erosion rate are given in *steadystate_10Be_20mMyr.mat* and *steadystate_26Al_20mMyr.mat*. Sea-level high-latitude ^{10}Be and ^{26}Al production rates in 1-cm depth increments below the surface are given in *P10.mat* and *P26.mat*. The file *er_half_Ma.mat* determines which set of bedrock profiles are beneath erosive warm-based ice (1) or non-erosive cold-based ice (0) at each time step.

Data availability. All data generated and analysed during this study are included in this Letter and its Supplementary Information. MATLAB forward-model code is available at https://github.com/shakunj/Bierman-et-al-2016-Nature.

30. Spratt, R. M. & Lisiecki, L. E. A Late Pleistocene sea level stack. *Clim. Past Discuss.* **11,** 3699–3728 (2015).
31. Clark, P. U. & Mix, A. C. Ice sheets and sea level of the last glacial maximum. *Quat. Sci. Rev.* **21,** 1–7 (2002).
32. Hemming, S. R., Bond, G. C., Broecker, W. S., Sharp, W. D. & Klas-Mendelson, M. Evidence from ^{40}Ar/^{39}Ar ages of individual hornblende grains for varying Laurentide sources of iceberg discharges 22,000 to 10,500 yr B.P. *Quat. Res.* **54,** 372–383 (2000).
33. Dowdeswell, J. A., Cofaigh, C. Ó., Andrews, J. T. & Scourse, J. D. Workshop explores debris transported by icebergs and paleoenvironmental implications. *Eos* **82,** 382–386 (2001).
34. Martin, T. & Wadhams, P. Sea-ice flux in the East Greenland Current. *Deep Sea Res. Part II* **46,** 1063–1082 (1999).
35. Bridgewater, D., Keto, L., McGregor, V. R. & Myers, J. S. in *Geology of Greenland* (eds Escher, E. & Watt, W. S.) 304–339 (Geological Survey of Greenland, 1976).
36. Larsen, H. C. Geological perspectives of the East Greenland continental margin. *Bull. Geol. Soc. Den.* **29,** 77–101 (1980).
37. Linthout, K., Troelstra, S. R. & Kuijpers, A. Provenance of coarse ice-rafted detritus near the SE Greenland margin. *Netherlands J. Geosci.* **79,** 109–121 (2000).
38. Spezzaferri, S. in *Proc. ODP Sci. Res.* Vol. 152 (eds Larsen, H. C., Saunders, A. & Clift, P. D.) 161–190 (Ocean Drilling Program, 1998).
39. Molnia, B. F. in *Glacial-Marine Sedimentation* (ed. Molnia, B. F.) 593–626 (Plenum, 1983).
40. Party, S. S. in *Proc. ODP Init. Rep.* Vol. 152 (eds Larsen, H. C., Saunders, A. & Clift, P. D.) 177–256 (Ocean Drilling Program, 1994).
41. Greve, R. Relation of measured basal temperatures and the spatial distribution of the geothermal heat flux for the Greenland ice sheet. *Ann. Glaciol.* **42,** 424–432 (2005).
42. Kaus, B. J. P. Heating glaciers from below. *Nat. Geosci.* **6,** 683–684 (2013).
43. Fyke, J. G., Sacks, W. J. & Lipscomb, W. H. A technique for generating consistent ice sheet initial conditions for coupled ice sheet/climate models. *Geosci. Model Dev.* **7,** 1183–1195 (2014).
44. MacGregor, J. A. *et al.* A synthesis of the basal thermal state of the Greenland Ice Sheet. *J. Geophys. Res.* **121,** 1328–1350 (2016).
45. Bierman, P., Marsella, K., Patterson, C., Davis, P. & Caffee, M. Mid-Pleistocene cosmogenic minimum-age limits for pre-Wisconsinan glacial surfaces in southwestern Minnesota and southern Baffin Island: a multiple nuclide approach. *Geomorphology* **27,** 25–39 (1999).
46. Nishiizumi, K. Preparation of ^{26}Al AMS standards. *Nucl. Instrum. Methods Phys. Res. B* **223/224,** 388–392 (2004).
47. Nishiizumi, K. *et al.* Absolute calibration of ^{10}Be AMS standards. *Nucl. Instrum. Methods Phys. Res. B* **258,** 403–413 (2007).
48. Chmeleff, J., Von Blanckenburg, F., Kossert, K. & Jakob, D. Determination of the ^{10}Be half-life by multicollector ICP-MS and liquid scintillation counting. *Nucl. Instrum. Methods Phys. Res. B* **268,** 192–199 (2010).
49. Korschinek, G. *et al.* A new value for the half-life of ^{10}Be by heavy-ion elastic recoil detection and liquid scintillation counting. *Nucl. Instrum. Methods Phys. Res. B* **268,** 187–191 (2010).
50. Corbett, L., Bierman, P. & Rood, D. Constraining multi-stage exposure-burial scenarios for boulders preserved beneath cold-based glacial ice in Thule, northwest Greenland. *Earth Planet. Sci. Lett.* **440,** 147–157 (2016).
51. Stone, J. Air pressure and cosmogenic isotope production. *J. Geophys. Res.* **105,** 23753–23759 (2000).
52. Argento, D., Reedy, R. & Stone, J. Modeling the earth's cosmic radiation. *Nucl. Instrum. Methods Phys. Res. B* **294,** 464–469 (2013).
53. Argento, D., Stone, J., Reedy, R. & O'Brien, K. Physics-based modeling of cosmogenic nuclides part II—key aspects of in-situ cosmogenic nuclide production. *Quat. Geochronol.* **26,** 44–55 (2015).
54. Borchers, B. *et al.* Geological calibration of spallation production rates in the CRONUS-Earth project. *Quat. Geochronol.* **31,** 188–198 (2016).
55. Lifton, N., Sato, T. & Dunai, T. J. Scaling in situ cosmogenic nuclide production rates using analytical approximations to atmospheric cosmic-ray fluxes. *Earth Planet. Sci. Lett.* **386,** 149–160 (2014).
56. Corbett, L. B. *et al.* Elevated cosmogenic 26-Al/10-Be production ratio at high latitude. *Eos* abstr. C53C–0739 (2016).
57. Party, S. S. in *Proc. Ocean Drilling Program* (eds Jansen, E., Raymo, M. E. & Blum, P.) 345–387 (Ocean Drilling Program, 1996).
58. Kohl, C. P. & Nishiizumi, K. Chemical isolation of quartz for measurement of *in-situ*-produced cosmogenic nuclides. *Geochim. Cosmochim. Acta* **56,** 3583–3587 (1992).
59. Corbett, L. B., Bierman, P. R. & Rood, D. H. An approach for optimizing in situ cosmogenic ^{10}Be sample preparation. *Quat. Geochronol.* **33,** 24–34(2016).
60. Rood, D. H., Brown, T. A., Finkel, R. C. & Guilderson, T. P. Poisson and non-Poisson uncertainty estimations of ^{10}Be/^{9}Be measurements at LLNL–CAMS. *Nucl. Instrum. Methods Phys. Res. B* **294,** 426–429 (2013).
61. Rood, D. H., Hall, S., Guilderson, T. P., Finkel, R. C. & Brown, T. A. Challenges and opportunities in high-precision Be-10 measurements at CAMS. *Nucl. Instrum. Methods Phys. Res. B* **268,** 730–732 (2010).
62. Xu, S., Freeman, S. P. H. T., Rood, D. H. & Shanks, R. P. Decadal ^{10}Be, ^{26}Al and ^{36}Cl QA measurements on the SUERC 5 MV accelerator mass spectrometer. *Nucl. Instrum. Methods Phys. Res. B* **361,** 39–42 (2015).
63. Cande, S. C. & Kent, D. V. Revised calibration of the geomagnetic polarity timescale for the Late Cretaceous and Cenozoic. *J. Geophys. Res.* **100,** 6093–6095 (1995).

64. Fukuma, K. in *Proc. ODP Sci. Res.* Vol. 152 (eds Saunders, A. D., Larsen, H. C. & Wise, S. W. Jr) 265–269 (Ocean Drilling Program, 1998).
65. Wei, W. in *Proc. ODP Sci. Res.* Vol. 152 (eds Saunders, A. D., Larsen, H. C. & Wise, S. W. Jr) 147–160 (Ocean Drilling Program, 1998).
66. Spezzaferri, S. in *Proc. ODP Sci. Res.* Vol. 152 (eds Saunders, A. D., Larsen, H. C. & Wise, S. W. Jr) 161–189 (Ocean Drilling Program, 1998).
67. Norris, T. L., Gancarz, A. J., Rokop, D. J. & Thomas, K. W. Half-life of ^{26}Al. *J. Geophys. Res.* **88,** B331–B333 (1983).
68. Carlson, A. E. *et al.* Earliest Holocene south Greenland ice sheet retreat within its late Holocene extent. *Geophys. Res. Lett.* **41,** 5514–5521 (2014).
69. Rohling, E. J. *et al.* Sea-level and deep-sea-temperature variability over the past 5.3 million years. *Nature* **508,** 477–482 (2014).
70. de Boer, B., Lourens, L. J. & van de Wal, R. S. W. Persistent 400,000-year variability of Antarctic ice volume and the carbon cycle is revealed throughout the Plio-Pleistocene. *Nat. Commun.* **5,** 2999 (2014).
71. de Vernal, A. & Hillaire-Marcel, C. Natural variability of Greenland climate, vegetation, and ice volume during the past million years. *Science* **320,** 1622–1625 (2008).
72. Dutton, A. *et al.* Sea-level rise due to polar ice-sheet mass loss during past warm periods. *Science* **349,** 153 (2015).
73. Elderfield, H. *et al.* Evolution of ocean temperature and ice volume through the mid-Pleistocene climate transition. *Science* **337,** 704–709 (2012).
74. Sosdian, S. & Rosenthal, Y. Deep-sea temperature and ice volume changes across the Pliocene-Pleistocene climate transitions. *Science* **325,** 306–310 (2009).
75. Hansen, J., Sato, M., Russell, G. & Kharecha, P. Climate sensitivity, sea level and atmospheric carbon dioxide. *Phil. Trans. R. Soc. Lond. A* **371,** http://dx.doi.org/10.1098/rsta.2012.0294 (2013).
76. Eldrett, J. S., Harding, I. C., Wilson, P. A., Butler, E. & Roberts, A. P. Continental ice in Greenland during the Eocene and Oligocene. *Nature* **446,** 176–179 (2007).
77. Tripati, A. K. *et al.* Evidence for glaciation in the Northern Hemisphere back to 44 Ma from ice-rafted debris in the Greenland Sea. *Earth Planet. Sci. Lett.* **265,** 112–122 (2008).
78. Nishiizumi, K. *et al.* In situ produced cosmogenic nuclides in GISP2 rock core from Greenland summit. *Eos* **77,** abstr. OS41B–10 (1996).
79. Willerslev, E. *et al.* Ancient biomolecules from deep ice cores reveal a forested southern Greenland. *Science* **317,** 111–114 (2007).
80. Reyes, A. V. *et al.* South Greenland ice-sheet collapse during Marine Isotope Stage 11. *Nature* **510,** 525–528 (2014).
81. Bennike, O. *et al.* A multi-proxy study of Pliocene sediments from Île de France, North-East Greenland. *Palaeogeogr. Palaeoclimatol. Palaeoecol.* **186,** 1–23 (2002).
82. Feyling-Hanssen, R. W., Funder, S. & Petersen, K. S. The Lodin Elv Formation; a Plio-Pleistocene occurrence in Greenland. *Bull. Geol. Soc. Den.* **31,** 81–106 (1983).
83. Bennike, O. *et al.* Early Pleistocene sediments on Store Koldewey, northeast Greenland. *Boreas* **39,** 603–619 (2010).
84. Knutz, P. C., Hopper, J. R., Gregersen, U., Nielsen, T. & Japsen, P. A contourite drift system on the Baffin Bay–West Greenland margin linking Pliocene Arctic warming to poleward ocean circulation. *Geology* **43,** 907–910 (2015).
85. Koenig, S. J. *et al.* Ice sheet model dependency of the simulated Greenland Ice Sheet in the mid-Pliocene. *Clim. Past* **11,** 369–381 (2015).
86. Lunt, D. J., Foster, G. L., Haywood, A. M. & Stone, E. J. Late Pliocene Greenland glaciation controlled by a decline in atmospheric CO_2 levels. *Nature* **454,** 1102–1105 (2008).
87. Solgaard, A. M., Reeh, N., Japsen, P. & Nielsen, T. Snapshots of the Greenland ice sheet configuration in the Pliocene to early Pleistocene. *J. Glaciol.* **57,** 871–880 (2011).
88. Dolan, A. M. *et al.* Using results from the PlioMIP ensemble to investigate the Greenland Ice Sheet during the mid-Pliocene Warm Period. *Clim. Past* **11,** 403–424 (2015).

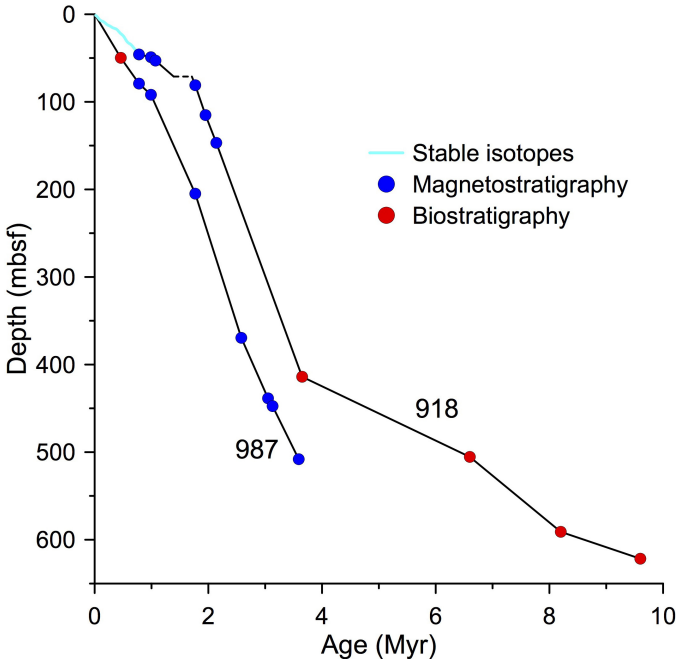

Extended Data Figure 1 | Age–depth models for Sites 918 and 987. Chronostratigraphic constraints[19,40] are identified by symbols. (mbsf, metres below seafloor.)

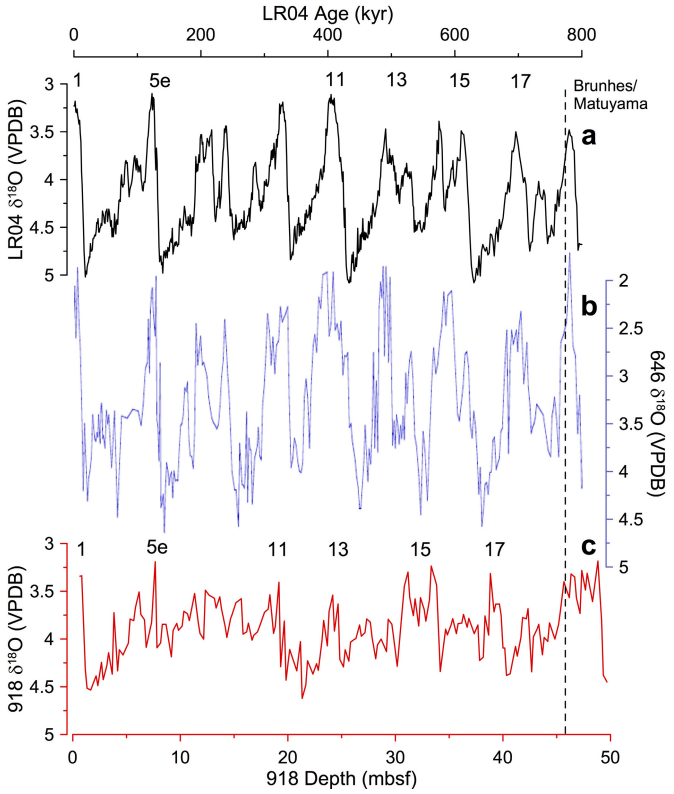

Extended Data Figure 2 | Site 918 planktonic $\delta^{18}O$ stratigraphy. a, The global benthic LR04 $\delta^{18}O$ stack on its timescale[20]. VPDB, Vienna Pee-Dee Belemnite standard. **b**, A planktonic (*N. pachyderma*, left-coiling) $\delta^{18}O$ record from ODP site 646 off southern Greenland, also on the global benthic $\delta^{18}O$ stack timescale[71]. **c**, The planktonic (*N. pachyderma*, left-coiling) $\delta^{18}O$ record from Site 918 on its depth scale. Notable interglacials in the LR04 stack and their interpreted correlatives at Site 918 are numbered, and the location of the Brunhes–Matuyama magnetic reversal in each record is denoted by the vertical dotted black line. The well resolved ODP site 646 $\delta^{18}O$ record is shown to provide a nearby planktonic record for comparison to Site 918.

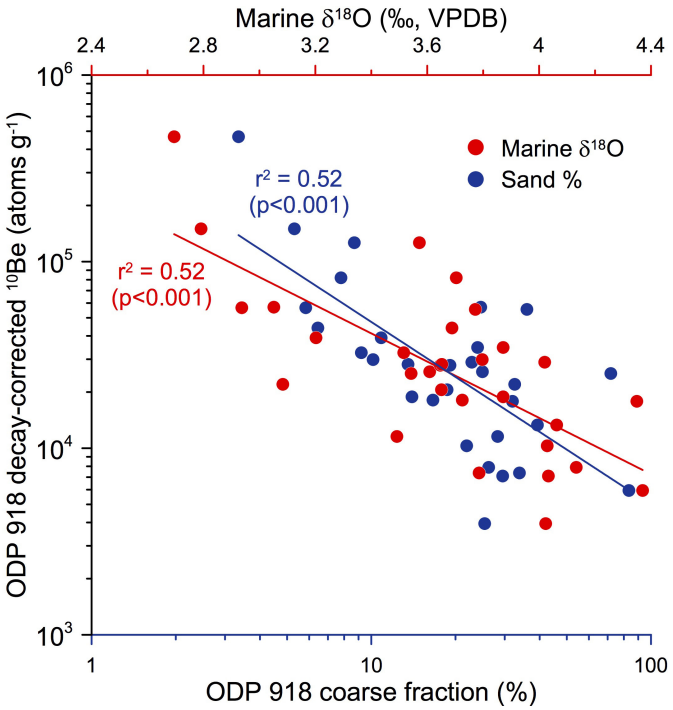

Extended Data Figure 3 | Comparing Site 918 decay-corrected ^{10}Be concentrations to Site 918 sand (>63 μm) concentrations and marine δ^{18}O over the past 7.5 Myr. All data have been binned to the same age intervals as the ^{10}Be data. Coarse fraction indicates sand. The r^2 and *P* values quantify the correlations of the ^{10}Be concentrations with the sand concentrations and marine δ^{18}O values.

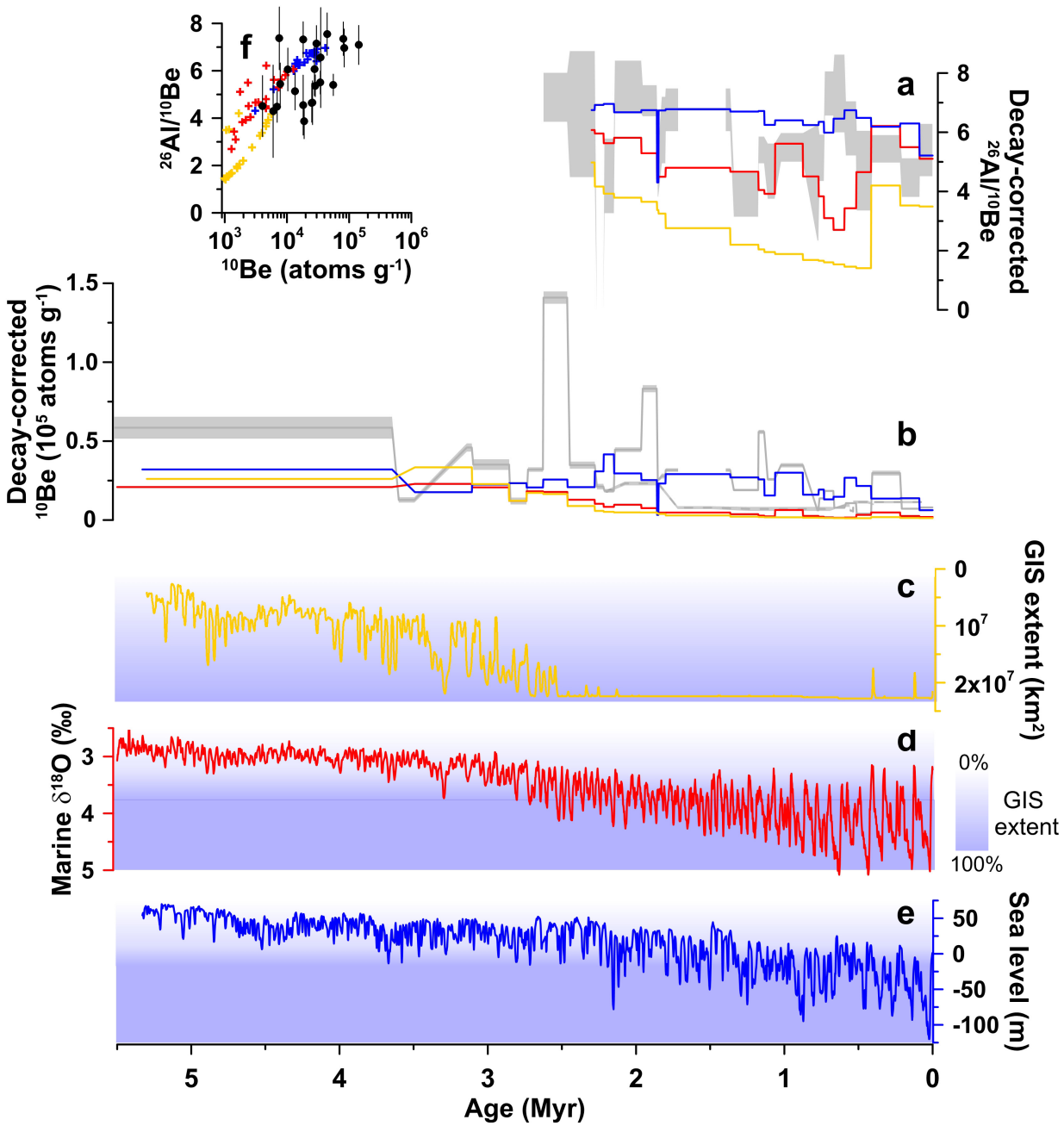

Extended Data Figure 4 | A simple forward model of Greenlandic cosmogenic-nuclide concentrations and ratios over the past 5 million years. a–e, Simulated (coloured lines) ^{26}Al/^{10}Be ratios (**a**) and ^{10}Be concentrations (**b**) of glacially eroded material from a box model with ice extent parameterized as a function of GIS extent from a full ice-sheet model[70] (**c**), marine δ^{18}O (ref. 20) (**d**), and sea level[69] (**e**). The colours of the simulated records in **a** and **b** correspond to the associated drivers of the model in **c**, **d** and **e**. The ice extent parameterization is represented by the blue shading in **c**, **d** and **e**. Sites 918 and 987 cosmogenic-nuclide records are shown by 1σ grey shading in **a** and **b**, and simulated records have been binned to the same resolution. **f**, ^{26}Al/^{10}Be–^{10}Be relationships in the simulated (colours) and ODP Site 918 (black) records. Error bars are 1σ. See Methods for model details and https://github.com/shakunj/Bierman-et-al-2016-Nature for computer code.

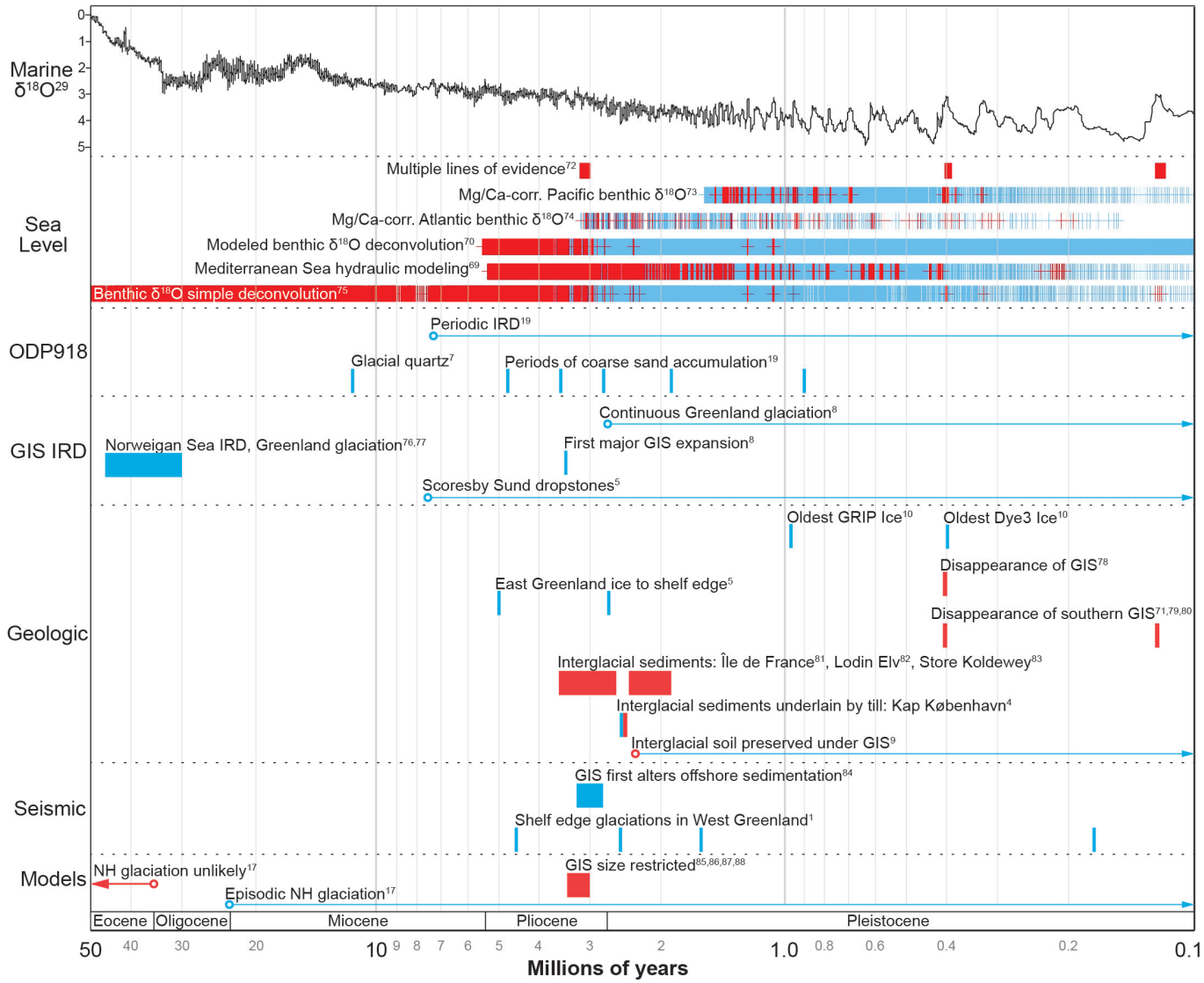

Extended Data Figure 5 | Fully referenced version of Fig. 2. NH, Northern Hemisphere. Data are from refs 1, 4, 5, 7–10, 17, 19 and 69–88.